High-order Verified Solutions of the 3D Laplace Equation

SHASHIKANT MANIKONDA, MARTIN BERZ and KYOKO MAKINO
Department of Physics and Astronomy
Michigan State University
East Lansing, MI 48824
USA
manikond@msu.edu, berz@msu.edu, makino@msu.edu http://bt.pa.msu.edu/

Abstract: For many practical problems, numerical methods to solve partial differential equations (PDEs) are required. Conventional finite element or finite difference codes have a difficulty to obtain precise solutions because of the need for an exceedingly fine mesh which leads to often prohibitive CPU time. While conventional methods exhibit such a difficulty, some practical problems even require solutions guaranteed. The Laplace equation is one of the important PDEs in physics and engineering, describing the phenomenology of electrostatics and magnetostatics among others, and various problems for the Laplace equation require highly precise and verified solutions.

We present an alternative approach based on high-order quadrature and a high-order finite element method utilizing Taylor model methods. An n-th order Taylor model of a multivariate function f consists of an n-th order multivariate Taylor polynomial, representing a high order approximation of the underlying function f, and a remainder error bound interval for verification, width of which scales in $(n+1)$ st order.

The solution of the Laplace equation in space is first represented as a Helmholtz integral over the two-dimensional surface. The latter is executed by evaluating the kernel of the integral as a Taylor model of both the two surface variables and the three volume variables inside the cell of interest. Finally, the integration over the surface variables is executed, resulting in a local Taylor model of the solution within one cell. Examples of the method will be given, demonstrating achieved accuracy with verification.

Key-Words: Laplace equation, PDE solver, Helmholtz method, verified computation, Taylor model, differential algebra, interval arithmetic.

1 Introduction

Many problems in physics and engineering require the solution of the three dimensional Laplace equation

$$\Delta\psi(\vec{r}) = 0 \text{ in the bounded volume } \Omega \subset \mathtt{R}^3 \quad (1)$$

It is well known that under mild smoothness conditions for the boundary $\partial\Omega$ of Ω, the Laplace equation admits unique solutions if either ψ or its derivative normal to $\partial\Omega$ are specified on the entire boundary surface $\partial\Omega$. In many typical applications, not only the normal derivative of ψ but indeed the entire gradient $\vec{\nabla}\psi$ is known on the surface; for example, in the magnetostatic case the entire field $\vec{B} = \vec{\nabla}\psi$ is measured, and not merely whatever component happens to be normal to the surface under consideration. The corresponding problem of determining ψ based on the knowledge of the field $\vec{\nabla}\psi(\vec{r}) = \vec{f}(\vec{r})$ on the surface $\partial\Omega$ is referred to as the Helmholtz problem.

Analytic closed form solutions for the 3D case can usually only be found for special problems with certain regular geometries where a separation of variables can be performed. However, in most practical 3D cases, numerical methods are the only way to proceed. Frequently the finite difference or finite element approaches are used to find the approximations of the solution on a set of points in the region of interest. But because of their relatively low approximation order, for the

problem of precise solution of partial differential equations (PDEs), the methods have very limited success because of the prohibitively large number of mesh points required. For reference, codes like the frequently used TOSCA [1, 2] can usually solve 3D Laplace problems with a relative accuracy of 10^{-4} with meshes of size about 10^{-6}[3]. Furthermore, direct solution verification of such methods is often very difficult.

In the following we develop a new method based on the Helmholtz theorem and the Taylor model methods[4, 5] utilizing the corresponding tools in the code COSY INFINITY [6, 7] to find a verified solution of the Laplace equation starting from the field boundary data. The final solution is provided as a set of local Taylor models, each of which represents an enclosure of a solution for a sub-box of the volume of interest.

2 Theory and Implementation

2.1 The Helmholtz Approach

We begin by representing the solution of the Laplace equation via the Helmholtz vector decomposition theorem [8, 9, 10, 11, 12, 13], which states that any vector field $\vec{B}$ which vanishes at infinity can inside an arbitrary boundary region Ω be written as the sum of two terms

$$\vec{B}\left(\vec{x}\right) = \vec{\nabla} \times \vec{A}_t\left(\vec{x}\right) + \vec{\nabla}\phi_n\left(\vec{x}\right), \tag{2}$$

where

$$\begin{aligned}\phi_n\left(\vec{x}\right) =& \frac{1}{4\pi}\int_{\partial\Omega} \frac{\vec{n}\left(\vec{x}_s\right)\cdot\vec{B}\left(\vec{x}_s\right)}{\left|\vec{x}-\vec{x}_s\right|} ds \\ &- \frac{1}{4\pi}\int_{\Omega} \frac{\vec{\nabla}\cdot\vec{B}\left(\vec{x}_v\right)}{\left|\vec{x}-\vec{x}_v\right|} dV \\ \vec{A}_t\left(\vec{x}\right) =& -\frac{1}{4\pi}\int_{\partial\Omega} \frac{\vec{n}\left(\vec{x}_s\right)\times\vec{B}\left(\vec{x}_s\right)}{\left|\vec{x}-\vec{x}_s\right|} ds \\ &+ \frac{1}{4\pi}\int_{\Omega} \frac{\vec{\nabla}\times\vec{B}\left(\vec{x}_v\right)}{\left|\vec{x}-\vec{x}_v\right|} dV.\end{aligned}$$

Here $\partial\Omega$ is the surface which bounds the volume Ω. $\vec{x}_s$ denotes points on the surface $\partial\Omega$, and $\vec{x}_v$ denotes points within Ω. $\vec{n}$ is the unit vector perpendicular to $\partial\Omega$ that points away from Ω, and $\vec{\nabla}$ denotes the gradient with respect to $\vec{x}_v$.

The first term is usually referred to as the solenoidal term, and the second term as the irrotational term. Because of the apparent similarity of these two terms to the well-known vector- and scalar potentials to $\vec{B}$, we note that in the above representation, it is in general not possible to utilize only one of them; for a given problem, in general both ϕ_n and $\vec{A}_t$ will be nonzero.

For the special case that $\vec{B} = \vec{\nabla}V$, we have $\vec{\nabla}\times\vec{B} = 0$; furthermore, if V is a solution of the Laplace equation $\Delta V = \vec{\nabla}^2 V = 0$, we have $\vec{\nabla}\cdot\vec{B} = 0$. Thus in this case, all the volume integral terms vanish, and $\phi_n\left(\vec{x}\right)$ and $\vec{A}_t\left(\vec{x}\right)$ are completely determined from the normal and the tangential components of $\vec{B}$ on the surface $\partial\Omega$ via

$$\begin{aligned}\phi_n\left(\vec{x}\right) &= \frac{1}{4\pi}\int_{\partial\Omega} \frac{\vec{n}\left(\vec{x}_s\right)\cdot\vec{B}\left(\vec{x}_s\right)}{\left|\vec{x}-\vec{x}_s\right|} ds \\ \vec{A}_t\left(\vec{x}\right) &= -\frac{1}{4\pi}\int_{\partial\Omega} \frac{\vec{n}\left(\vec{x}_s\right)\times\vec{B}\left(\vec{x}_s\right)}{\left|\vec{x}-\vec{x}_s\right|} ds.\end{aligned}$$

For any point within the volume Ω, the scalar and vector potentials and consequently the solution of the Laplace equation depend only on the field on the surface $\partial\Omega$.

Using the fact that if $\vec{x} \neq \vec{x}_s$, we have $\vec{\nabla}\left(1/\left|\vec{x}-\vec{x}_s\right|\right) = -\left(\vec{x}-\vec{x}_s\right)/\left|\vec{x}-\vec{x}_s\right|^3$, and similar relationships, it is possible to explicitly obtain the gradient of the scalar potential, and with some more work the curl of the vector potential; the results have the explicit form

$$\begin{aligned}&\vec{\nabla}\phi_n\left(\vec{x}\right) \\ &= -\frac{1}{4\pi}\int_{\partial\Omega} \frac{\left(\vec{x}-\vec{x}_s\right)\left(\vec{n}\left(\vec{x}_s\right)\cdot\vec{B}\left(\vec{x}_s\right)\right)}{\left|\vec{x}-\vec{x}_s\right|^3} ds \end{aligned} \tag{3}$$

$$\begin{aligned}&\vec{\nabla}\times\vec{A}_t\left(\vec{x}\right) \\ &= \frac{1}{4\pi}\int_{\partial\Omega} \frac{\left(\vec{x}-\vec{x}_s\right)\times\left(\vec{n}\left(\vec{x}_s\right)\times\vec{B}\left(\vec{x}_s\right)\right)}{\left|\vec{x}-\vec{x}_s\right|^3} ds. \end{aligned} \tag{4}$$

From (2) we know that the field inside the volume of interest is just a sum of the irrotational and the solenoidal part, (3) and (4) respectively.

This is then the solution for the magnetic field as surface integrals. But to numerically integrate the kernel and get the verified solution as the local Taylor model we need a specialized numerical scheme. In the following subsections we introduce one such scheme based on the Taylor models[4, 5] of the code COSY INFINITY[6, 7]. First, we introduce the definition of the Taylor model and the antiderivation operation on the Taylor models which will be extensively used in implementation of the scheme. We then proceed to explain the numerical scheme to perform the surface integration.

2.2 Taylor Models and the Antiderivation

Let us begin with the definition of Taylor models.

Definition (Taylor Model) *Let $f : D \subset R^v \longrightarrow R$ be a function that is $(n+1)$ times continuously partially differentiable on an open set containing the v-dimensional domain D. Let x_0 be a point in D and P the n-th order Taylor polynomial of f around x_0. Let I be an interval such that*

$$f(x) \in P(x - x_0) + I \text{ for all } x \in D$$

and that has the property that I scales with the $(n+1)$st power of the width of D. Then we call the pair (P, I) an n-th order Taylor model of f around x_0 on D.

A full theory of Taylor model arithmetic for elementary operations, intrinsic functions, initial value problems and functional inversion problems has been developed; see [5, 4, 14, 15] and references therein. A verified implementation of Taylor models and the arithmetic operations exists in the code COSY INFINITY[6, 7] having the Taylor polynomial coefficients represented by floating point numbers, and the details about the implementation can be found in [16, 4].

For the purposes of the further discussion, one particular "intrinsic" function, the so-called antiderivation, plays an important role. We note that a Taylor model for the integral with respect to variable i of a function f can be obtained from the Taylor model (P, I) of the function by merely integrating the part P_{n-1} of order up to order $n-1$ of the polynomial, and bounding the n-th order into the new remainder bound[5, 14, 15].

Specifically, we define the antiderivation operation ∂_i^{-1} on an n-th order Taylor model (P, I) as

$$\partial_i^{-1}(P, I) = \left(P_{\partial_i^{-1}}, I_{\partial_i^{-1}}\right) = \left(\int_0^{x_i} P_{n-1}(x)\, dx_i, \left(B\left(P - P_{n-1}\right) + I\right) \cdot B(x_i)\right).$$

Here $B\left(P - P_{n-1}\right)$ is a bound for the part of P that is of exact order n, and $B(x_i)$ is an interval bound for the variable x_i obtained from the range of definition of x_i.

With this definition, a bound for a definite integral with respect to the variable x_i from x_{il} to x_{iu} both in the domain of validity of the Taylor model (P, I) enclosing a function f can be obtained as

$$\int_{x_{il}}^{x_{iu}} f dx_i \in \left(P_{\partial_i^{-1}}|_{x_i = x_{iu} - x_{i0}} - P_{\partial_i^{-1}}|_{x_i = x_{il} - x_{i0}}, I_{\partial_i^{-1}}\right).$$

2.3 Solution of the Helmholtz Problem using Taylor Models

In this subsection, we develop a verified method to determine sharp enclosures of the field $\vec{B}$ and the potential ψ with the Helmholtz method. Utilizing Taylor model arithmetic introduced above, the following algorithm now allows to solve the Laplace equation for the Helmholtz problem.

Algorithm

1) Discretize the surface $\partial\Omega$ into individual surface cells S_i with centers s_i and the volume Ω into volume cells V_j with centers v_j.

2) Pick a volume cell V_j.

3) For each surface cell S_i, evaluate the integrands (3) and (4), the so-called "kernels", in Taylor model arithmetic to obtain a Taylor model representations in **both** the surface variables of S_i **and** the volume variables of V_j, i.e. in a total of five variables.

4) Use the Taylor model antiderivation operation twice to perform integration over the surface variables of each cell S_i.

5) Add up all results to obtain a three dimensional Taylor model enclosing the field $\vec{B}$ over the volume cell V_j.

6) If a verified enclosure of the potential ψ to $\vec{B}$ over the volume cell V_j is desired, integrate the Taylor model represented field $\vec{B}$ over any path using the Taylor model antiderivation operation.

As a result, for each of the volume cells V_j, Taylor model enclosures for the fields $\vec{B}$ and potentials ψ are obtained. All the mathematical operations to evaluate these Taylor models and surface integration are implemented using the Taylor model tools available in the code COSY INFINITY[6, 7].

Apparently the computational expense scales with the product of the number of volume elements and the number of surface elements; of these, the number of volume elements is more significant because of their larger number. In practice one observes that when using high-order Taylor models, a rather small number of volume elements is required, in particular compared to the situation in conventional field solvers discussed earlier.

3 An Example: the Bar Magnet

3.1 The Example Field

As a reference problem to study the behavior of the method, we consider the magnetic field of rectangular iron bars of a uniformly magnetized material with inner surfaces ($y = \pm y_0$) parallel to the mid-plane $y = 0$ as shown in Fig. 1. The geometry of these uniformly magnetized bars, which are assumed to be infinitely extended in the $\pm y$ directions, is defined by: $x_1 \leq x \leq x_2, |y| \geq y_0$, and $z_1 \leq z \leq z_2$. From this bar magnet one can obtain an analytic solution for the magnetic field $\vec{B}(x, y, z)$ [17, 18, 19], and the result is given by

$$B_y(x, y, z) = \frac{B_0}{4\pi} \sum_{i,j=1}^{2} (-1)^{i+j} \left[\arctan\left(\frac{X_i \cdot Z_j}{Y_+ \cdot R_{ij}^+} \right) + \arctan\left(\frac{X_i \cdot Z_j}{Y_- \cdot R_{ij}^-} \right) \right]$$

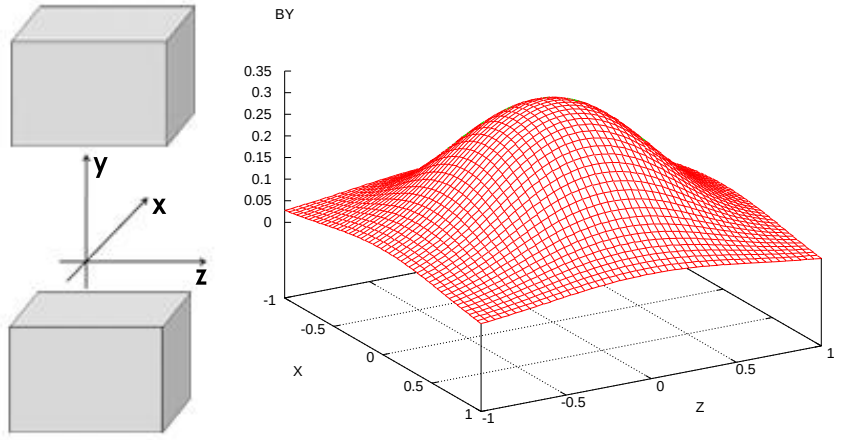

(a) (b)

Figure 1: (a) Geometric layout of the bar magnet, consisting of two bars of magnetized material. (b) Magnetic field B_y on the center plane ($y = 0$) of the bar magnet. $B_0 = 1$ Tesla and the interior of this magnet is defined by $-0.5 \leq x \leq 0.5$, $-0.5 \leq y \leq 0.5$, and $-0.5 \leq z \leq 0.5$.

$$B_x(x,y,z) = \frac{B_0}{4\pi}\sum_{i,j=1}^{2}(-1)^{i+j}\left[\ln\left(\frac{Z_j+R_{ij}^-}{Z_j+R_{ij}^+}\right)\right]$$
$$B_z(x,y,z) = \frac{B_0}{4\pi}\sum_{i,j=1}^{2}(-1)^{i+j}\left[\ln\left(\frac{X_j+R_{ij}^-}{X_j+R_{ij}^+}\right)\right] \quad (5)$$

where $X_i = x - x_i, Y_\pm = y_0 \pm y, Z_i = z - z_i$, and $R_{ij}^\pm = \sqrt{X_i^2 + Y_j^2 + Z_\pm^2}$, and B_0 specifies the field strength.

3.2 Setup of Example Computations

As an example case, we define a test bar magnet by $[x_1, x_2] = [-0.5, 0.5]$, $[z_1, z_2] = [-0.5, 0.5]$, $y_0 = 0.5$ and $B_0 = 1$ Tesla. The y component of the magnetic field, B_y, of the test bar magnet on the center plane $y = 0$ is shown in Fig. 1.

According to the recipe described in the previous section, we performed the magnetic field and the magnetic potential computations with verification. The program coded in COSY language[6], enabling the full usage of Taylor model arithmetic, was run on a Pentium IV, 2 GHz, 512 MB Ram, Linux machine with COSY INFINITY compiled using the GNU Fortran compiler.

First we will see the performance of the method at the step 4), then at the step 5), as described in the algorithm.

3.3 Analysis on Surface Element Discretization

As a first step in the analysis of the influence of the discretization of the surface and volume on the result, we study the contributions of the surface elements towards the Taylor model remainder interval part of the total integral. The volume expansion point is chosen as $\vec{r} = (0.1, 0.1, 0.1)$, avoiding the trivial choice of $(0, 0, 0)$ where all the odd order terms in the expressions of the bar magnet (5) vanish. The size of the volume box around the volume expansion point is chosen zero. Thus after the surface integration, the polynomial part of the dependence on volume vanishes except for the constant term, and the accuracy is only limited by the width of the surface element, which after integration over the surface variables influences the width of the remainder bound.

We plot the width of the remainder interval versus surface element length for the scalar potential ψ for different orders of computation in Fig. 2. Here the center of the surface element is chosen as $\vec{r}_s = (0.034, 0.011, 0.5)$, more or less randomly. It is observed that for high orders, the method quickly reaches an accuracy of around 10^{-16} for about 2^5 surface subdivisions, which correspond to about $2^{10} \approx 1000$ surface element cells per surface. Under the assumption that each of these surface cells brings a similar contribution, the accuracy due to the surface discretization will be in the range of approximately $6 \cdot 1000 \cdot 10^{-16} < 10^{-12}$.

3.4 Analysis on Volume Element Discretization

We now study the dependency of the polynomial part and width of the remainder interval of the magnetic field on the volume element length. Now the surface element length is kept fixed at 1/128. Fig. 3 shows the remainder interval width for B_y versus volume element lengths for different orders of computation. The other components of the magnetic field B_x and B_z exhibit a similar behavior.

We see that a verified accuracy in the range of 10^{-4} can be achieved for a volume element width of around 10^{-1}, corresponding to a total of around 1000 volume elements. This number compares very favorably to the earlier mentioned numbers for the commercial code TOSCA [1, 2]. An accuracy in the range of 10^{-7} can be achieved for a width of around $10^{-1.4}$, corresponding to a total of around $200,000$ volume elements. The typical computation time for such 8th order computations is about 1000 seconds in the above mentioned computational environment.

4 Conclusion

Overall, we see that the method of simultaneous surface and volume expansion of the Helmholtz

integrals leads to verified tools for the solutions of PDEs which when executed in Taylor model arithmetic can lead to very sharp enclosures. It is obvious that the method can be generalized to other surface-integral based approaches to the solution of PDEs.

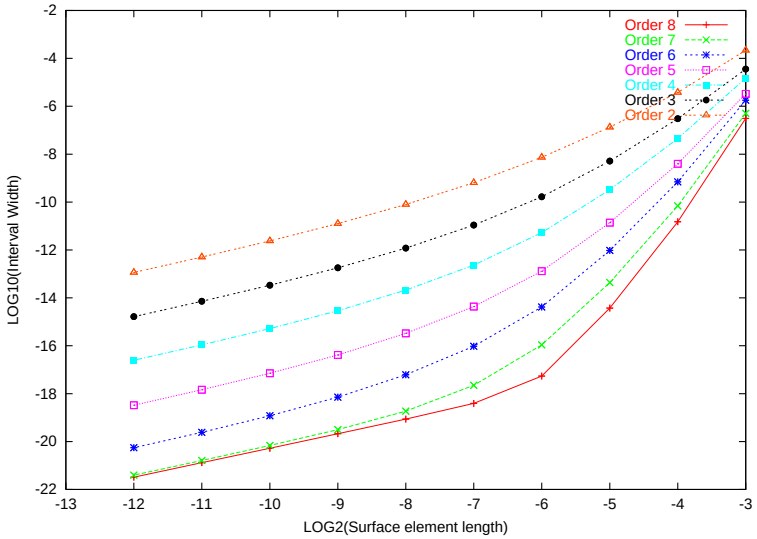

Figure 2: Remainder interval width (vertically in $\log_{10}$) versus surface element length (horizontally in $\log_2$) for integration for the scalar potential ψ over a single surface element and vanishing volume size.

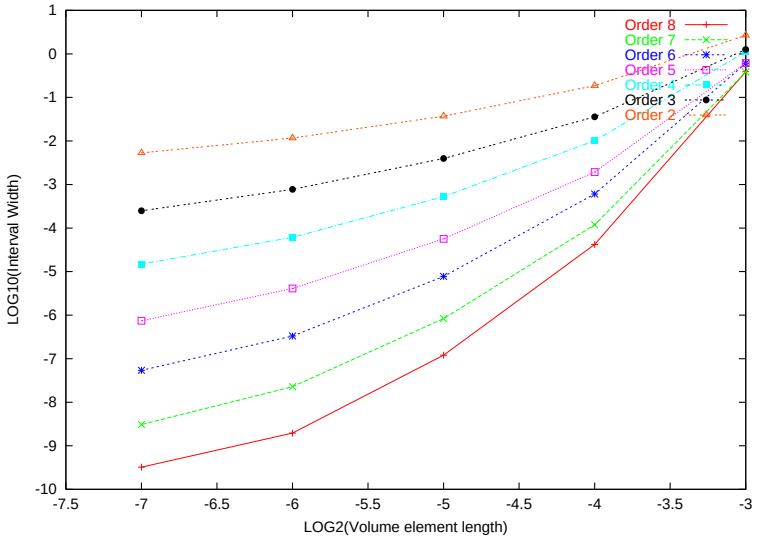

Figure 3: Remainder interval width (vertically in $\log_{10}$) versus length of volume element (horizontally in $\log_2$) for B_y.

References:

[1] The TOSCA reference manual. Technical report, Vector Fields Limited, 24 Bankside, Kidlington, Oxford, OX5 1JE, England.

[2] The TOSCA user guide. Technical report, Vector Fields Limited, 24 Bankside, Kidlington, Oxford, OX5 1JE, England.

[3] W. Wan. Private communication.

[4] K. Makino and M. Berz. Taylor models and other validated functional inclusion methods. *International Journal of Pure and Applied Mathematics*, 6,3:239–316, 2003. http://bt.pa.msu.edu/pub.

[5] K. Makino. *Rigorous Analysis of Nonlinear Motion in Particle Accelerators*. PhD thesis, Michigan State University, East Lansing, Michigan, USA, 1998. Also MSUCL-1093.

[6] M. Berz, J. Hoefkens, and K. Makino. COSY INFINITY Version 8.1 - programming manual. Technical Report MSUHEP-20703, Department of Physics and Astronomy, Michigan State University, East Lansing, MI 48824, 2002. See also http://cosy.pa.msu.edu.

[7] M. Berz and K. Makino. COSY INFINITY Version 8.1 - user's guide and reference manual. Technical Report MSUHEP-20704, Department of Physics and Astronomy, Michigan State University, East Lansing, MI 48824, 2002. See also http://cosy.pa.msu.edu.

[8] P. M. Morse and H. Feshbach. *Methods of Theoretical Physics, Part I and II*. 1953.

[9] P.L.Walstrom. Soft-edged magnet models for higher-order beam-optics map codes. *Nucl. Instrum. Meth.*, A519, Issues 1-2:216–221, 2004.

[10] M. Venturini, D. Abell, and A. Dragt. Map computation from magnetic field data and application to the LHC high-gradient quadrupoles. *eConf*, C980914:184–188, 1998.

[11] P. Walstrom, A. Dragt, and T. Stasevich. Computation of charged-particle transfer maps for general fields and geometries using electromagnetic boundary-value data. Particle Accelerator Conference (PAC2001), 2001.

[12] M. Venturini and A. Dragt. Computing transfer maps from magnetic field data. Particle Accelerator Conference (PAC 99), 1999.

[13] M. Venturini and A. J. Dragt. Accurate computation of transfer maps from magnetic field data. *Nucl. Instrum. Meth.*, A427:387–392, 1999.

[14] M. Berz and K. Makino. Verified integration of ODEs and flows using differential algebraic methods on high-order Taylor models. *Reliable Computing*, 4(4):361–369, 1998.

[15] M. Berz and K. Makino. New Methods for High-Dimensional Verified Quadrature. *Reliable Computing*, 5(1):13–22, 1999.

[16] N. Revol, K. Makino, and M. Berz. Taylor models and floating-point arithmetic: Proof that arithmetic operations are validated in COSY. *Journal of Logic and Algebraic Programming*, in print, 2004. University of Lyon LIP Report RR 2003-11, MSU Department of Physics Report MSUHEP-30212, http://bt.pa.msu.edu/pub.

[17] M. M. Gordon and T. Taivassalo. The z^4 orbit code and the focusing bar fields used in beam extraction calculations for superconducting cyclotrons. *Nuclear Instruments and Methods*, 247:423, 1986.

[18] R. Degenhardt and M. Berz. High accuracy description of the fringe field in particle spectrographs. *Nuclear Instruments and Methods*, A427:151–156, 1999.

[19] M. Berz. *Modern Map Methods in Particle Beam Physics*. Academic Press, San Diego, 1999. Also available at http://bt.pa.msu.edu/pub.